The Journal of Experimental Biology **198**, 2441–2452 (1995)
Printed in Great Britain © The Company of Biologists Limited 1995
JEB9681

MAXIMUM SINGLE LEG FORCE PRODUCTION: COCKROACHES RIGHTING ON PHOTOELASTIC GELATIN

R. J. FULL, A. YAMAUCHI* AND D. L. JINDRICH
Department of Integrative Biology, University of California at Berkeley, Berkeley, CA 94720, USA

Accepted 8 August 1995

Summary

Integrating studies of mechanics, neural control and isolated muscle function are possible using arthropod legs. To evaluate leg performance, we measured the ground reaction forces generated by individual legs of the six-legged cockroach *Blaberus discoidalis* (3.1 g), during an emergency behavior, righting or over-turning. We used a photoelastic method to measure the forces generated by individual legs simultaneously. A gelatin track placed between crossed polarizing filters was illuminated from below, and a high-speed video camera recorded the stress-induced optical signals from above. The size and skew of the optical patterns were found to be related to the magnitude and direction of the force. We discovered that the ground reaction forces generated during the righting behavior of the death-head cockroach were eight times greater than those observed during high-speed running, supporting the possibility that relative leg forces (leg force per unit body weight) during running and maximal leg activity differ more in small arthropods than in larger vertebrates. Non-geometric scaling of relative leg force (i.e. scaling to less than body mass$^{-0.33}$), along with the reduced force-generating ability of a single leg in animals with many legs, may help to explain why the maximum relative leg force production by six-legged cockroaches, as well as by some other small insects, can be similar to the relative single leg forces produced by two- and four-legged vertebrates that are almost 1000 times more massive. Leg number and body mass alone, however, appear to be insufficient to explain the variation observed in relative leg force production at a given body mass, because enormous diversity in musculo-skeletal parameters exists. The maximal relative leg force of the cockroach *B. discoidalis* during righting was at the low end of a 100-fold variation observed for smaller insects wedging (pushing through a small crevice) and pulling loads. Thus, this cockroach can be characterized as a moderately strong insect with the capacity for relatively high speed. Results from the present study question the predictive strength of the simple geometric scaling arguments involving a strength:weight ratio as they are applied to small arthropods and encourage further consideration of the importance of leg number, muscle force production and mechanical advantage in the derivation of general principles of leg performance.

Key words: locomotion, mechanics, muscle, insects, arthropods, cockroach, *Blaberus discoidalis.*

Introduction

Integrating studies of locomotor mechanics, neural control and isolated muscle function remains a challenge. By using a tractable musculo-skeletal system, the arthropod leg, we can address this problem through two complementary approaches: direct measurement of performance and computer modeling. One parameter of particular importance is the ability of an animal to generate maximum leg force. In the present study, we selected an emergency behavior, righting or over-turning, that we speculated was complex and likely to result in higher levels of force production than high-speed running. Specifically, we hypothesized that the maximum ground reaction forces during righting exceed those during high-speed running in insects. We examined the leg force production data available for running, considered the various relationships that have been proposed to apply to leg force production, and attempted to develop a framework within which arthropod leg performance can be compared with that of other species.

We chose to study the leg performance of the death-head cockroach *Blaberus discoidalis* because much is already known about the animal's biomechanics (Full and Tu, 1990; Full *et al.* 1994; Ting *et al.* 1994) and metabolic energetics (Full and Tullis, 1990; Herreid and Full, 1984). In particular, single leg ground reaction force data during running are already available (Full *et al.* 1991).

The forces that a single leg of an animal experiences during running increase with body mass. Because the increase in ground

*Present address: Department of Bioengineering, 2480 MEB, University of Utah, Salt Lake City, UT 84112, USA.

reaction force tends to be directly proportional to body mass, leg forces can be remarkably similar multiples of body weight for animals that differ in body mass. Legs of bipedal birds and mammals that differ 10 000-fold in body mass produce forces 2.3–2.5 times body weight (Blickhan and Full, 1993).

Leg force relative to body weight decreases as the number of legs used in terrestrial locomotion increases (Blickhan and Full, 1993). The greater leg number of arthropods, therefore, tends to make relative leg forces during running lower than for vertebrates. Animals with six or more legs have a greater opportunity to distribute peak ground reaction forces than bipeds and quadrupeds. Since the average force over one cycle of leg movements during running must be equal to body weight, the peak force on any one leg of a many-legged animal can be reduced if a greater number of legs make contact with the ground. Blickhan and Full (1993) have shown that hexapedal trotters (i.e. insects and crabs) generate half of the relative leg force of four-legged trotters and only a quarter of the force observed in hopping and running bipeds. Rapidly running cockroaches, for example, produce forces equivalent to half of their body weight with each of their six legs during a stride (Full *et al.* 1991).

We therefore suspect that maximum leg force production in insects is not attained during running, as may be the case for some large mammals or birds. We anticipate that the reduction in relative leg force production that results from a cockroach possessing six legs, rather than fewer, is more than compensated by the scaling advantage of a small body mass.

An animal's maximum relative force production has been argued to increase as body mass decreases (Alexander, 1985). Small animals produce smaller absolute forces than larger animals. However, if small animals are geometrically similar to large animals (i.e. if area is proportional to the square of the linear dimension and mass is proportional to the cube of the linear dimension), then we would expect small animals to generate greater relative leg forces than large animals. If force is proportional to cross-sectional area and body mass is proportional to volume, then as the area (including muscle cross-sectional area) -to-volume ratio increases in progressively smaller animals, relative force production should also increase. Legendary reports of amazingly high strength-to-weight ratios in arthropods, such as ants, support this prediction, as do data from studies on beetles (Evans, 1977; Evans and Forsythe, 1984).

We hypothesize that relative leg forces during running and maximal leg activity will differ more in small arthropods than in larger vertebrates, depending upon leg number and the scaling of maximum leg force production per body weight.

To investigate our hypotheses, we measured leg force production during running and during an activity that, we proposed, was more likely to result in maximum leg force production, righting. Selecting a behavior that both may elicit maximal performance and would be useful for future comparative studies was difficult. The behaviors used to evaluate performance are often dictated by the ease of developing a suitable laboratory performance test rather than by the characteristics of the behavior itself. Complex, three-dimensional, dynamic and unpredictable behaviors are not usually selected first. Unfortunately, these may be the very behaviors that reveal the most about leg function. Many complex behaviors that are appropriate for study, such as climbing, turning, maneuvering, negotiating obstacles and righting, have been ignored because of the difficulty in determining the three-dimensional kinetics and kinematics of motion. Adequate measurements of arthropod leg performance have also proved to be technically difficult (Bennet-Clark, 1975; Blickhan and Barth, 1985; Cruse, 1976; Full *et al.* 1991; Katz and Gosline, 1993; Klarner *et al.* 1986; Queathem and Full, 1995). To measure leg force production during righting in cockroaches, we continued the development of a unique technique employing photoelastic gelatin (Harris and Ghiradella, 1980; Harris, 1978). Photoelastic methods permit simultaneous measurement of individual leg forces for complex, unpredictable behaviors.

Materials and methods

Animals

We used the death-head cockroach *Blaberus discoidalis* (Serville) in our experiments. The mean mass of the animals used was 3.1±0.6 g (mean ± S.D., N=14). Cockroaches were individually housed in plastic containers and given dog food and water *ad libitum.*

General theory

Photoelastic principles were used to measure ground reaction forces. A generalized photoelastic unit consists of two elements: polarized light and a photoelastic material. Polarized light may be produced by passing ordinary light through a polarizing filter. A second polarizing filter placed in the light path will absorb all light components that are not parallel to its polarizing axis. If the second filter is placed so that its polarizing axis is perpendicular to that of the polarized light, the filter will completely absorb the light (Fig. 1A). If, however, the polarized light is rotated, any component of the light parallel to the second filter's polarizing axis will pass through the filter. The degree of rotation will determine the magnitude of the component that passes through the second filter (Fig. 1B).

An applied force stresses a photoelastic material, causing it to rotate the axis of polarized light to a degree dependent on the magnitude of the applied force. Therefore, when a stressed material is placed between two polarizing filters aligned with their axes perpendicular, the intensity of the emergent light will be proportional to the degree of rotation of the light, which in turn will be proportional to the force applied to the material. By relating the emerging optical signal to known forces applied to the photoelastic material, it is possible to determine the magnitudes of unknown forces.

Apparatus

The apparatus used, consisting of a photoelastic unit, a track, video image-capturing equipment and computer image analysis software (Fig. 2), was based on the general photoelastic method described by Harris (1978). The

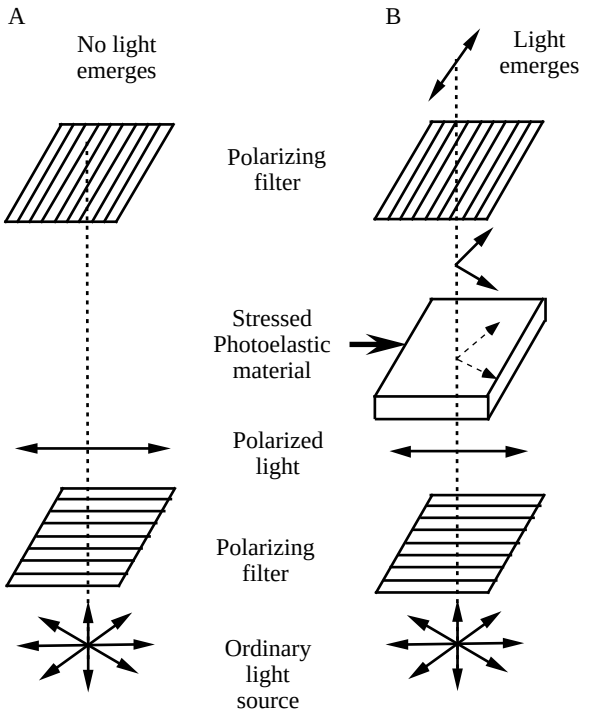

Fig. 1. Theory of the photoelastic force platform. (A) When a pair of polarizing filters is arranged with their polarizing axes at right angles, no light from the source will emerge from a second filter. (B) If a photoelastic material (e.g. gelatin) placed between the filters is stressed, the axis of light will be rotated. The light emerging from the second filter can, therefore, be related to the stress acting on the material.

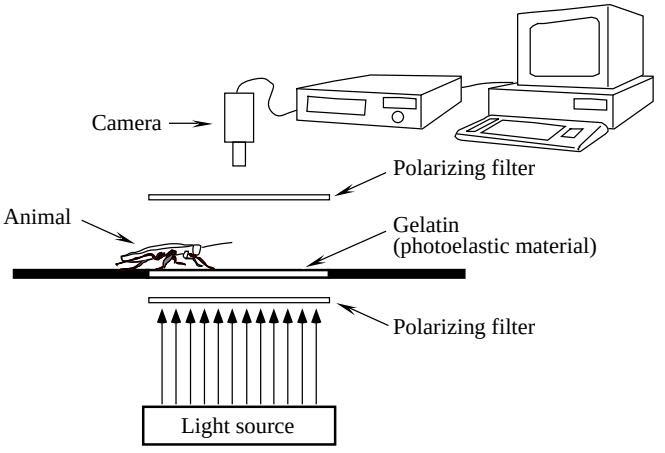

Fig. 2. Photoelastic force platform. The experimental apparatus consisted of a gelatin slab fitted into a track, placed between a pair of polarizing filters with perpendicular axes, and a light source. A video camera above the top filter recorded the emerging light. The camera and video recorder were attached to a computer (Apple Macintosh), which was used for image capture, storage and analysis. For further details see text.

photoelastic unit consisted of a thin slab of gelatin placed between a pair of orthogonally crossed polarizing filters. We used a polarizing sheet for the lower filter (Polaroid HN38S linear polarizer) and either a similar sheet or a camera-mounted (Edmund Scientific photo mount polarizing filter) filter for the upper filter. The lower filter was positioned with its polarizing axis parallel to the long axis of the gelatin slab and the upper filter was positioned with its axis perpendicular to the long axis of the gelatin slab. A 300-bloom gelatin (Sigma, from porcine skin) was used to produce a 15 % solution, which was poured into a glass-plate mold and allowed to set at room temperature, before refrigeration storage at 5 °C (see Harris, 1978, for the gelatin-preparation technique). The mold was a 10.2 cm×30.5 cm well with a glass bottom and 0.32 cm thick glass or Plexiglas plates forming the sides. The well was completely filled with gelatin so that the surface of the gelatin was level with the top surface of the side plates. After the gelatin had set, the mold was placed into the track, polarizing filters were positioned above and below it, and a light source was placed below the entire unit (Fig. 2). We employed two types of uniform-intensity light sources in our experiments: an overhead projector lamp and a 15 W fluorescent lamp placed in a parabolic reflector. The fluorescent lamp was used when it was important to minimize heat-induced softening of the gelatin.

We used a Plexiglas track that was 96.5 cm long and 10.2 cm wide (Fig. 2). In position, the gelatin plate lay in the middle of the track, level with the surrounding surface and forming part of the track floor. The entire track plus the gelatin plate was raised at least 15 cm above the ground to accommodate the light source.

The trials were video-taped from above at 1000 frames s^{-1} using a high-speed camera with an image intensifier (Kodak Ektapro 1000). Video-taped segments were then transferred to computer files using a frame-grabbing board and software (Neotech Image Grabber, NUBus). The images were analyzed on a computer (Macintosh) using image analysis software (Image 1.14, NIH, and the Ultimage Concept V.i., Graftek, France, package for LabVIEW 2.2.1, National Instruments).

Measurement of optical patterns

Prior to analysis, stress-induced optical patterns on the gelatin must be recorded, isolated from 'noise' in the gelatin plate and divided into four quadrants whose cumulative areas and intensities could be measured. Images captured from NTSC format video had a resolution of 640×480 pixels (or bytes), each with a gray value ranging from zero (black) to 255 (white). We measured the cumulative area and intensity of a given region of the digitized image using the computer image analysis software described above. Initially, we used Image 1.14 from NIH for analysis; however, we later developed our own image-analysis software using the Ultimage Concept V.i. package for LabVIEW (National Instruments), considerably expediting the analysis of multiple images.

To measure the cumulative areas and intensities of the quadrants of an optical pattern, a threshold function was first applied to the image to isolate the pattern from background noise and to delineate the edges of the pattern. A threshold

function sets pixels with values outside a specified range to zero. Pixels with values within the range retain their original values. All of the images collected during one experimental session with a given gelatin slab were thresholded to the same range to ensure that the analysis was consistent between the calibration measurements and experimentally produced force measurements. For the experiments described here, a threshold with a lower value of 100 and an upper value of 255 was used. The pattern was then divided into four separate regions, and the cumulative area and intensity of a region were determined by summing the cumulative value of the pixels in the region (intensity) and the number of pixels in the region with values greater than zero (area). Although, in principle, either area or intensity measurements may be used, for these experiments we chose to use area measurements for our analysis. Intensity measurements are more sensitive to the arrangement of the recording apparatus, can easily be washed out and are more difficult to extrapolate when part of the pattern has been obscured. If each gelatin plate is calibrated independently, as we recommend because of variation between preparations, and the positions of the gelatin and the camera are not changed between the calibration and the measurement of experimentally produced forces, measuring the relative areas (i.e. in units of pixels) of the patterns produced during the calibration and the experiment is sufficient to measure forces.

To measure an optical signal produced by a cockroach, it was often necessary to reduce noise around the pattern and/or to fill in areas of the pattern that were obscured by the leg of the animal. Fig. 3A shows a captured image of a cockroach during righting behavior, with the optical pattern isolated and enlarged in Fig. 3B. Extrapolating regions of the pattern is made possible by the bilateral symmetry of each lobe of the pattern about its midline (the 45° line extending from the center of the pattern through the lobe). Generally, this was carried out by manually setting pixels in the image to values greater than zero and estimating the size of the lobes. In the future, we may use simple symmetry algorithms incorporated in the LabVIEW program where such extrapolation is necessary. Once the pattern had been cleared of noise (by manually removing bright spots in the image caused by irregularities on the gelatin surface) and any obscured regions had been filled (Fig. 3C), we were able to measure the areas of the individual lobes of the patterns by counting the number of pixels with values greater than zero (Fig. 3D).

Force calibrations

In engineering studies, photoelastic models are analyzed to determine the state of stress at each point in a model. In two-dimensional studies, stress is applied to the model in the plane perpendicular to the direction of viewing. Three-dimensional studies are usually conducted by stressing the model in three perpendicular planes, ‘freezing’ the stressed model, then slicing it into slabs that can be studied two-dimensionally (Dally and Riley, 1991). Two aspects of animal ground reaction forces precluded the use of standard photoelastic techniques for their analysis: the contact area was usually obscured by the leg of the animal, and the forces involved were three-dimensional and dynamic. This made it necessary to study the optical pattern formed around the area of contact rather than to calculate the retardation of the polarized light passing through the gelatin *at* the contact area. Induced stress causes the region surrounding the contact area to become optically active. By studying the optical patterns caused by induced stress, it was possible to obtain information about the forces acting at the contact area.

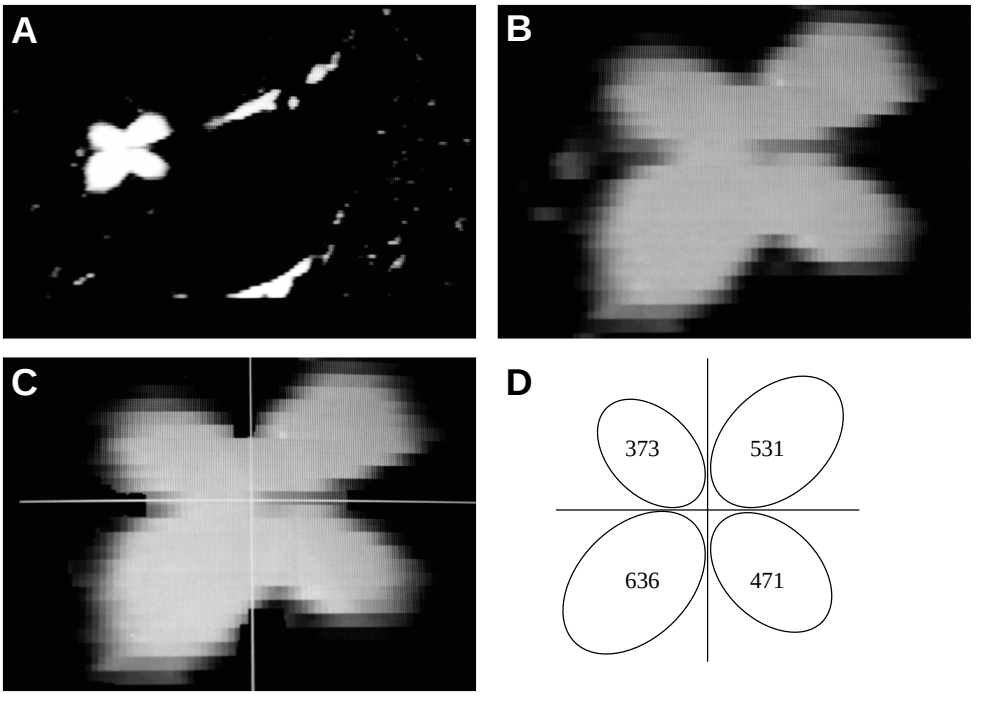

Fig. 3. Images used to analyze the cockroach righting behavior. (A) Image taken from high-speed video. (B) Enlarged image of optical signal after ‘capture’ into a computer analysis system using frame-grabbing software and hardware. (C) Thresholded image that has been divided into four quadrants. (D) The cumulative areas measured for the four quadrants shown in C, i.e. sum of pixels with gray level (intensity) values greater than zero.

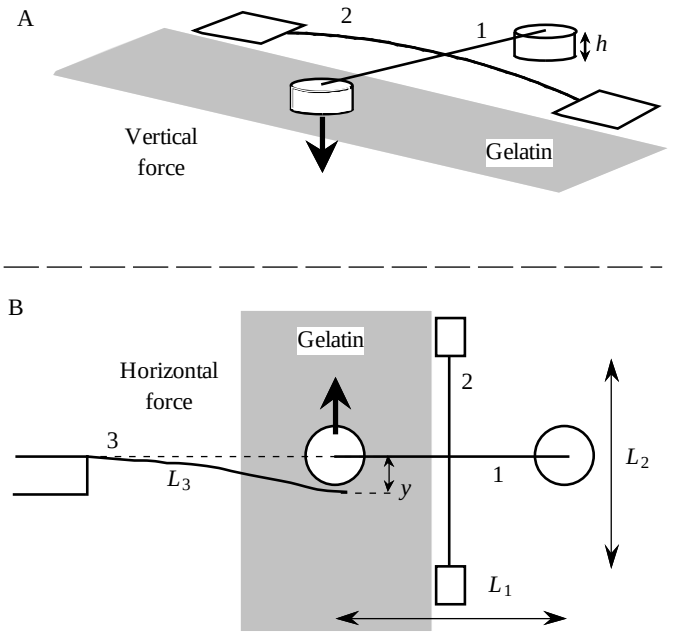

Fig. 4. Apparatus used to calibrate the photoelastic force platform. (A) Calibration forces in the vertical direction were produced by deflecting a wire (1) attached to a hex-nut (height, h=2 mm) which rested on the surface of the gelatin. A second wire (2) was placed across the first, perpendicular to it, so that the midpoints of both wires were in contact. Both ends of wire 2 were attached to the base adjacent to the force platform, producing deflections of both wires. (B) Calibration forces in the horizontal direction were produced by deflecting a third wire (3), which touched the hex-nut as shown, by a distance y. L_1, L_2 and L_3 are the lengths of wires 1, 2 and 3 and were 0.05 m, 0.06–0.12 m and 0.1 m, respectively.

Horizontal and vertical force calibration along the polarizing axes

We determined the relationship between applied force and the resulting optical signal. Forces were produced by deflecting thin brass wires that were connected to a contact area on the gelatin surface, a 2 mm diameter hex-nut (Fig. 4A). Hex-nuts were glued to both ends of a 0.5 mm diameter brass wire (wire 1). This wire (wire 1; 0.05 m in length) was placed perpendicular to the edge of the gelatin, so that the hex-nut at one end rested on the gelatin and the other nut rested on the surrounding glass plate. A second wire (wire 2; 0.06–0.12 m in length) was placed perpendicularly on top of the first wire, so that the midpoints of both wires were in contact (Fig. 4). The ends of the second wire were attached to the level plate surface (not to the gelatin) at points equal distances from the midpoint. Deflections in both wires produced a vertical force at the contact area with a magnitude that depended on the distance between the attachment points. The wires were considered to be center-loaded beams, fixed at both ends, for analysis. A horizontal force was produced by deflecting the end of a third wire (wire 3) against the side of the contact hex-nut (Fig. 4B). Wire 3 was attached to a micromanipulator at a point 10 cm from its tip, so that its deflection could be accurately measured. This wire was considered to be a cantilever beam, loaded at the end, for analysis. We tested the stiffness of the wire over the range of deflections used in these calibrations and found that the modulus of elasticity did not vary appreciably.

The forces at the contact area are given by:

$$\text{vertical force} = 96EIh/(L_1^3 + L_2^3), \quad (1)$$

$$\text{horizontal force} = 3EIy/L_3^3, \quad (2)$$

where E is the modulus of elasticity of the brass wires, h is the height of hex-nut contact, y is the deflection of wire 3 and L_1, L_2 and L_3 are the lengths of wires 1, 2, and 3, respectively. I is the area moment of inertia, and is given by:

$$I = \pi R^4/4, \quad (3)$$

where R is the radius of the wire.

The optical pattern resulting from a force stressing the surface of the gelatin appears as a bright 'clover-shaped' spot of light (Fig. 3A–C). A pair of mutually perpendicular dark bands divides the light spot into four quadrants (I–IV) or 'leaves'. Each dark band corresponds to the polarizing axis of one of the polarizing filters. We found that the area and the intensity of the optical signal increased as the vertical force or horizontal (frictional) forces were increased. Horizontal forces are taken to be the force component oriented in the surface plane. When a vertical force only was applied, the resulting pattern was symmetrical. All quadrants had approximately equal intensity and area (Fig. 5A). A horizontal force, applied in the direction of one of the polarizing axes, caused the signal to skew in the direction of the force, i.e. the quadrants that lie in the direction of the applied force became larger than the quadrants in the opposite direction (Fig. 5B).

We quantified the relationship between applied stress and optical signal by varying the magnitudes of the vertical and horizontal forces, F_v and F_h (and hence the stresses, σ_v and σ_h, respectively), and measuring their effects on the optical signal. Contrary to the contention of Harris and Ghiradella (1980) that the area of the optical signal should depend only on σ_v, we found that the total brightness and area depended on both σ_h and σ_v. This finding prevented us from simply measuring σ_v by calibrating it to the total area of the optical pattern.

By applying a series of vertical and horizontal stresses, each aligned with one of the polarizing axes, we obtained a calibration curve in which the area of the largest two quadrants of the optical signal relative to the area of the whole signal (which we term the quadrant ratio) varied linearly with the ratio of horizontal stress to the total stress (σ_h/σ_t, where total stress is σ_t: Fig. 5C). Total stress, as we define it in this calibration, is simply the sum of the vertical and horizontal stresses ($\sigma_v+\sigma_h=\sigma_t$) and is not meant to reflect the resultant stress. Since the fraction of σ_t made up by σ_v is simply $1-\sigma_h/\sigma_t$, measuring the relative area of the largest two quadrants allowed us to determine both the horizontal and vertical components of the applied stress. However, this

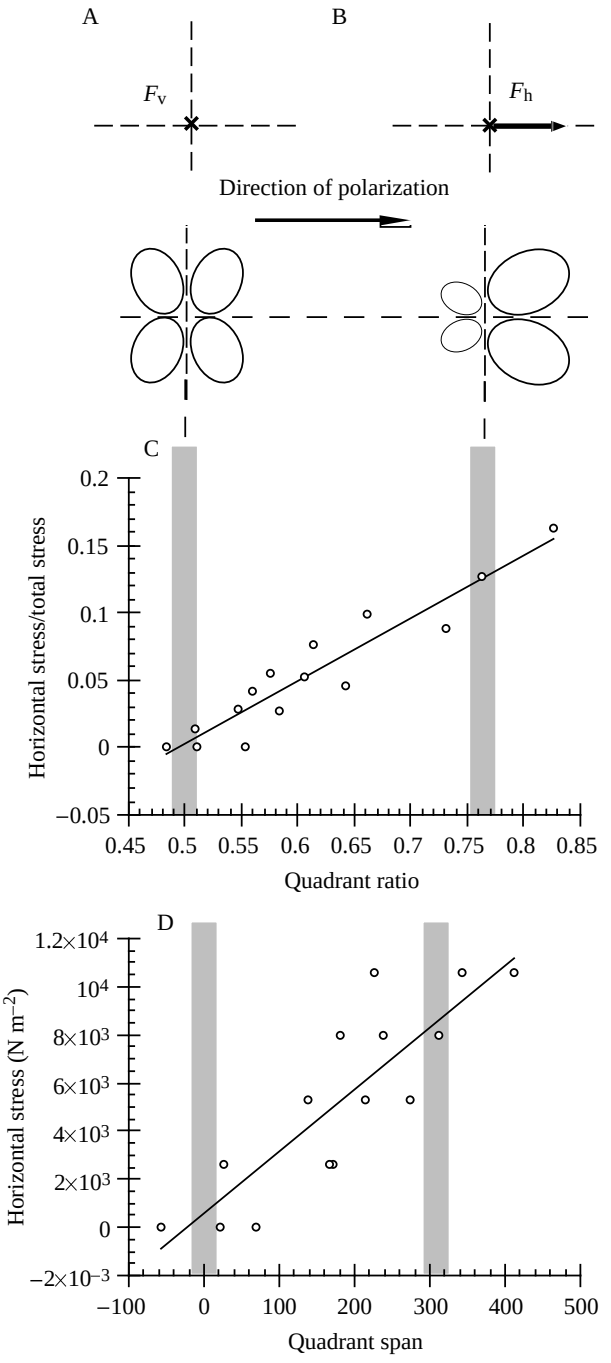

Fig. 5. Calibration along the polarizing axes. (A) A representation of an optical signal produced by light emerging from polarizing filter when the gelatin was stressed by a vertical force, F_v. The **x** represents a force going into the page. The pattern is a bright spot of light made up of four 'leaves' or quadrants. The dark lines between the 'leaves' were produced along the polarizing axis of each filter. (B) The pattern produced when the gelatin was stressed by a horizontal force, F_h, in the same direction as the polarizing axis of one filter. The arrow shows the direction of the applied force. (C) The relationship between the ratio of horizontal stress to total stress and the quadrant ratio, defined as the ratio of the two largest quadrants to the total area of the optical pattern. Horizontal stress/total stress = 0.46(quadrant ratio) − 0.23 (r=0.94). Shaded bars indicate the measured values of the patterns depicted in A and B. (D) The relationship between the horizontal stress and the quadrant span, defined as the sum of the areas of the two largest quadrants minus the sum of the areas of the two smallest quadrants. Horizontal stress = 26(quadrant span) + 588 (r=0.85). The relationships derived in C and D allow the separation of vertical and horizontal force components. Shaded bars indicate the measured values of the patterns depicted in A and B.

calibration provided only relative values for the stress components. To measure the absolute magnitude of an applied stress, it was necessary to be able to relate the horizontal stress component, the vertical component or the total stress directly to the optical signal. We found that the difference in area between the two largest quadrants and the two smallest quadrants (the quadrant span) varied linearly with the horizontal stress, σ_h alone (Fig. 5D). From these calibrations, we are able to measure σ_h and its proportion of σ_t directly and, hence, to calculate σ_t and σ_v.

However, these calibrations apply only to horizontal stresses in the direction of one of the polarizing axes. To measure the forces produced by a moving animal, it is necessary to establish not only their magnitude, but also their direction. It was, therefore, necessary to establish a relationship between the direction of an applied stress and the resulting optical pattern.

Direction of applied force

To measure the effect that a change in the direction of an applied stress had on the optical pattern produced, we constructed an apparatus which allowed us to rotate the direction of an applied force of known horizontal and vertical components (Fig. 6). The apparatus reflected a compromise between this requirement and the need to minimize obstruction of the optical pattern by the calibration apparatus. The system was similar to that used by Harris (1978) and consisted of an element angled against a fixed vertical wall. The magnitude of the horizontal and vertical forces produced depended on both the weight of the apparatus and the angle of inclination. The force-producing element consisted of a thin, rigid steel wire to which a thread was attached, from the center of which were hung various weights. This design differed from that of Harris (1978) in several important respects. First, contact at the wall was horizontal, rather than normal, to the force-producing element and the exact point of contact between the element and the vertical wall could be determined. Second, the system was nearly frictionless, except at the point of contact between the apparatus and the gelatin.

The relationship between the angle of force application (θ) and the optical pattern produced is illustrated in Fig. 7 for a force of constant magnitude. The shape of the pattern was quantified by measuring the area of each of the four quadrants, as described above. The area of the quadrant containing the direction of the applied force remained constant as the angle of force application varied. The areas of the adjacent quadrants

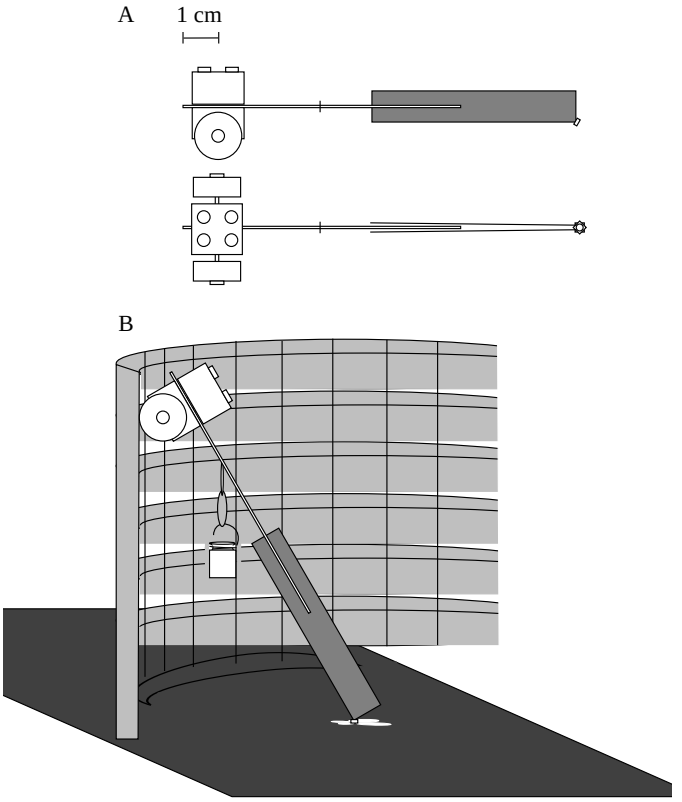

Fig. 6. Apparatus used to derive a model relating the shape of an optical pattern to the direction of applied horizontal force. (A) The apparatus consisted of a thin, steel wire from which weights were hung, a small wheeled 'cart' that approximated a frictionless contact point when rested against a vertical wall, a 2 mm hex-nut contact point, and two darkened half-coverslips connecting the steel wire to the contact point (to minimize interference with the pattern). (B) The apparatus rested against the inside wall of a 11 cm high × 13 cm diameter Plexiglas cylinder. The angle of the horizontal force was changed by resting the apparatus at different points around the circumference of the cylinder.

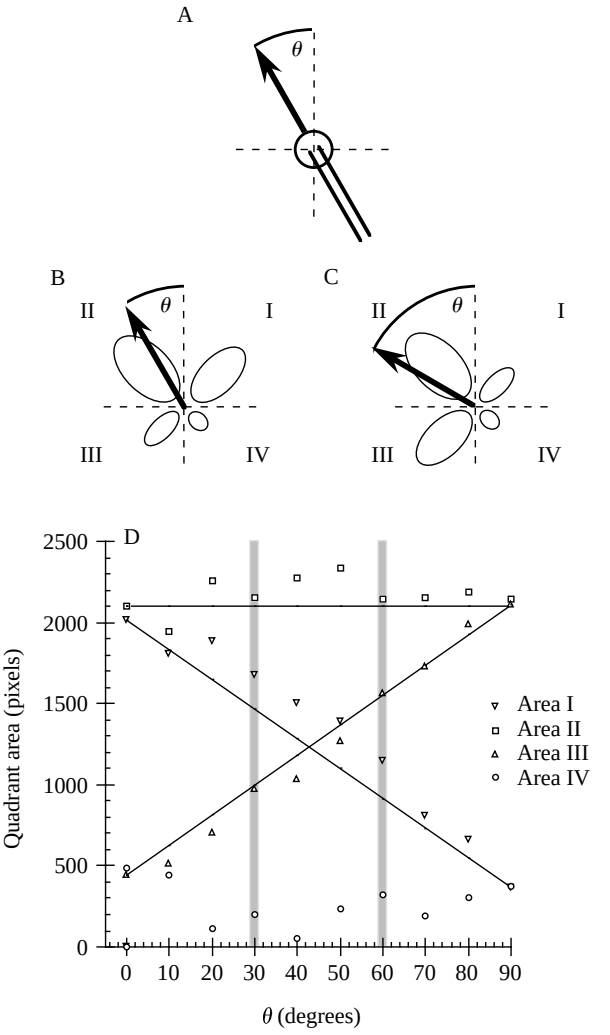

Fig. 7. Directional calibration of the optical signal produced by the photoelastic force platform. (A) Point of force application. The angle of the force component in the horizontal plane from the polarizing axis is shown by θ. (B) Depiction of an optical pattern for a horizontal force oriented at 30°. Quadrants are labelled I–IV. (C) Depiction of an optical pattern produced when the same horizontal force component is oriented at θ=60°. (D) The relationship between quadrant area and θ for each of the four quadrants (areas I–IV). The lines represent the predicted quadrant areas calculated from the measured areas at θ=0° using equations 4, 5 and 6 derived to relate quadrant area to rotation of the horizontal force (see text). Shaded bars indicate the measured quadrant areas of the patterns depicted in B and C.

increased or decreased as linear functions of θ. The changes in the area (a) of each quadrant were modeled using the following relationships:

$$a_{\mathrm{I}} = a_{\mathrm{II}} - [\theta(a_{\mathrm{II}} - a_{\mathrm{IV}*})/90], \quad (4)$$

$$a_{\mathrm{II}} = \text{constant}, \quad (5)$$

$$a_{\mathrm{III}} = [\theta(a_{\mathrm{II}} - a_{\mathrm{IV}*})/90)] + a_{\mathrm{IV}*}, \quad (6)$$

where θ is the angle between the force direction and the vertical polarizing axis (in degrees), a_{I} is the area of quadrant I, a_{II} is the area of quadrant II, a_{III} is the area of quadrant III, and $a_{\mathrm{IV}*}$ is the area of quadrant IV when θ=0°.

Note that we arranged the polarizing filters so that their axes were always parallel and perpendicular to the longitudinal plane of the gelatin plate. Changing the orientation of the filters was found to significantly affect the quadrant areas.

Horizontal and vertical force determination from an optical pattern

It is possible to determine the degree of rotation of any applied horizontal force from the polarizing axis by solving the quadrant area equations given above for θ:

$$\theta = [90(a_{\mathrm{II}} - a_{\mathrm{I}})]/(a_{\mathrm{II}} - a_{\mathrm{IV}*}). \quad (7)$$

Since the horizontal component of a force produced by a cockroach was not usually aligned with a polarizing axis, it

was necessary to calculate the predicted size of the equivalent optical pattern at a horizontal force rotation of 0° in order to calculate the magnitudes of the horizontal and vertical forces. We defined a_{II} to be the largest quadrant in any measured pattern. When σ_h is directed along one of the polarizing axes, the line of the polarizing axis between quadrant II and the largest adjacent quadrant is, therefore, defined as 0° (Fig. 7C).

Since the force calibrations were conducted at 0°, where an optical pattern is symmetrical about the polarizing axis parallel to the direction of applied force (Fig. 5), it was sufficient to calculate the equivalent areas of only two quadrants: one from the larger half of the pattern and one from the smaller. Since in the model a_{II} is constant, the measured area of a_{II} was taken as the value for one of the larger quadrants when calculating experimentally produced forces. The equivalent area at 0° of one of the smaller quadrants can be determined by measuring a_{IV*}. Since a_{IV*} is often obscured by the leg of the cockroach, it can also be solved for:

$$a_{IV*} = a_I + a_{III} - a_{II}. \quad (8)$$

From the values obtained for a_{II} and a_{IV*}, the quadrant span and the quadrant ratio can be determined:

$$\text{quadrant span} = 2(a_{II} - a_{IV*}), \quad (9)$$

$$\text{quadrant ratio} = 2a_{II}/2(a_{II} + a_{IV*}). \quad (10)$$

In Fig. 5C,D calibration relationships between the quadrant ratio and σ_h/σ_t and between the quadrant span and the horizontal stress were established for θ=0°. The coefficients of these relationships could be used to calculate the magnitudes of the stresses acting on the gelatin:

$$\sigma_h/\sigma_t = M_1(\text{span}) + \text{intercept}_1, \quad (11)$$

$$\sigma_h = M_2(\text{ratio}) + \text{intercept}_2, \quad (12)$$

$$\sigma_v = [\sigma_h/(\sigma_h/\sigma_t)] - \sigma_h, \quad (13)$$

where M_1 and intercept_1 are the slope and intercept of the relationship between the quadrant ratio and σ_h/σ_t (Fig. 5C), and M_2 and intercept_2 are the slope and intercept of the relationship between the quadrant span and σ_h (Fig. 5D). Forces can then be determined by multiplying the calculated stresses by the area of contact.

Leg contact area

To calculate peak force magnitudes from calculated stress values, we estimated leg contact area. We used a video camera (Kodak Ektapro camera with Nikon Micro-Nikkor 105 mm lens; 0.012 mm per pixel resolution) to obtain highly magnified images of the cockroach leg contacting the ground. We measured the area of contact, assumed to be the tarsal pads, using a computer program (NIH Image 1.41). The contact areas were 0.77±0.11 mm^2 (S.D.) for the middle leg and 0.97±0.03 mm^2 (S.D.) for the hind leg (N=3). The analysis methods used are most accurate for defined point areas in the range 0.5–2 mm^2. Larger contact areas were found to obscure the light pattern, and irregular contact areas resulted in non-clover-leaf shapes that are problematic to analyze.

Time response

Finally, we tested whether the optical pattern produced by the gelatin was sensitive to the length of time over which the forces were applied. If the gelatin is perfectly elastic, as this analysis assumes, its response to stress will be instantaneous. If, however, the gelatin acts viscoelastically, the response to stress will depend on time. To test the time response, we applied forces over very short time intervals (3–6 ms) and compared the resulting signals with those produced by forces applied over longer periods (>3 s). We dropped small metal balls (approximately 1 mm diameter) onto the gelatin to produce short-interval forces and recorded the resulting optical patterns with a high-speed video camera (1000 frames s^{-1}; Kodak EktraPro 1000). We compared the resulting optical pattern with those produced when a long-interval force was applied, using the calibration method described above. The optical response of the gelatin was not reduced by the use of short-interval forces, indicating that gelatin can be considered to be elastic over the time intervals used in the present study.

Procedure

It was necessary to calibrate each gelatin plate to determine the relationships described in Fig. 5, because the optical patterns produced in response to stress varied among different gelatin preparations. We assumed that each gelatin plate had the same optical response over its entire area, and that errors due to heterogeneity within the gelatin or to edge effects were relatively small.

To examine the forces produced by a running cockroach, an animal was placed on the track and prodded until it ran across the gelatin surface at a nearly constant speed (compared at several intervals during the trial). Each animal was run five or six times with short rest periods between each trial. Trials in which an animal did not run in a straight line or at a constant speed were rejected. The animals did not appear to have any difficulty in running over the gelatin surface; they were not observed to slip or to stick to the surface. To measure the ground reaction forces produced during righting behavior, an animal was turned over onto its dorsum and placed on the gelatin surface. We filmed the animal until it righted. Each individual was used in 5–6 trials, with 5 min rest periods between trials. Trials during which an animal stopped attempting to right itself were rejected. Each gelatin plate was used for experiments during a single day only, since after 3–4 h the gelatin had softened and debris from the air and left by the animal began to interfere with the recording of the optical patterns.

Optical signals corresponding to the largest forces produced were selected for analysis. To measure force production during running, we selected signals produced in the middle step of a hind leg, where peak force production is likely to occur (Full *et al.* 1991). We also measured the time course of single leg force production during running by analyzing several sequential frames. Time to half peak force production was comparable with that measured with a force platform (Full *et al.* 1991), confirming the adequacy of the optical response time

of the gelatin. For the experiments on righting behavior, we selected the largest optical signals. In all cases, the brightest and clearest optical signals were chosen.

Results

Running

Behavior

The average speed of animals during the running trials was $28\pm3\,cm\,s^{-1}$ (S.D.; N=6). Animals ran in a straight line but, as in previous studies using a force platform, it was very difficult to obtain trials in which the animal moved at a constant average speed. Optical signals were obtained for all legs, but the clearest signals were obtained from the hind legs (Fig. 8A).

Ground reaction forces

Ground reaction forces during running were similar in pattern and relative magnitude to those obtained for this species using a force platform (Full *et al.* 1991). The front legs were used for deceleration of the body, while the hind legs were used for acceleration. The middle leg was used for deceleration during the first half of the step and acceleration during the latter half. All ground reaction vectors were aligned axially along the legs towards the body of the animal.

Ground reaction forces in the vertical direction (0.017 N) and vertical force per unit body weight (0.49) were both similar to those reported in a previous study on running using a force platform (Full *et al.* 1991). Horizontal forces measured using the photoelastic technique were also comparable with those using a force platform, despite the differences in body weight between the two studies. However, the larger animals in the present study moved at speeds that were $10\,cm\,s^{-1}$ slower than the smaller animals used in the earlier study (Full *et al.* 1991).

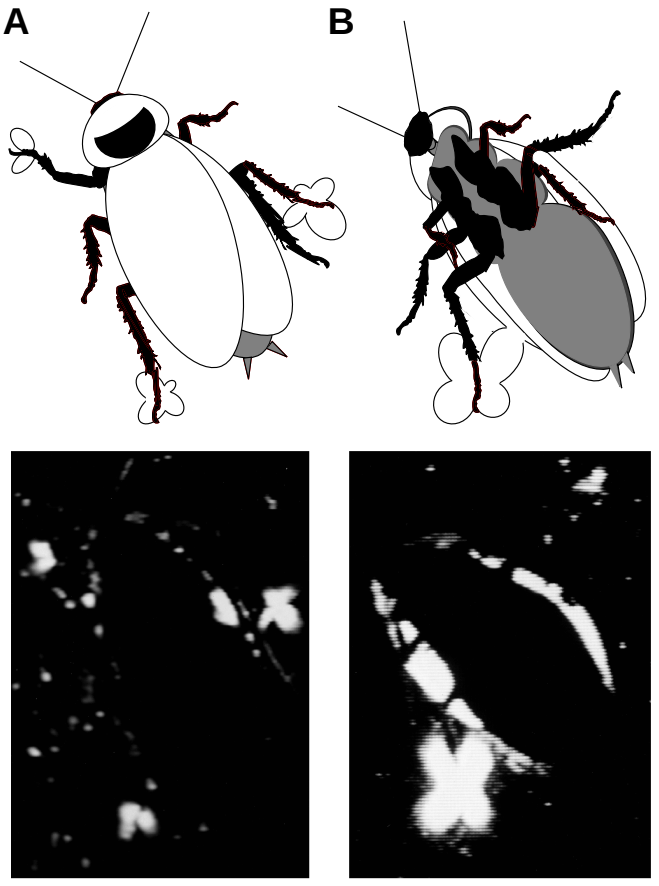

Fig. 8. The optical patterns produced during (A) a running trial and (B) a righting attempt. Note that the larger area of the patterns in B shows that righting produces forces that are much larger than the forces produced during running. The bright area that surrounds the body does not represent an applied force, but is a result of rotation of light due to the material properties of the wings and pronotum.

Righting

Behavior

Righting behavior was complex, dynamic and unpredictable. When upside-down, cockroaches struggled to regain normal orientation relative to the substratum. Failed attempts at righting were frequent and often resulted in the body simply rotating about a point near its center of mass. The legs, wings and body were often all involved in successful righting, but no single strategy can adequately characterize the behavior. Successful righting involving rotation about the longitudinal axis of the body often included curling the body and twisting the thorax in the direction of the final roll. Legs on the side furthest from the substratum flailed, and their inertia may have aided the rotation. The hind leg on the side over which the animal rolled was frequently attached to the gelatin as an anchoring point and underwent repeated extension and flexion at the coxa–femur joint. When the middle leg became attached to the gelatin, it appeared to extend at the coxa–femur joint as well as to rotate away from the body at the coxa. The middle and hind legs repeatedly generated large optical signals whether the righting attempt was successful or not (Fig. 8B).

Ground reaction forces

Cockroaches produced optical patterns of suitable quality for analysis using the photoelastic technique. The clear patterns suggested that the legs were making single-point contact with the gelatin. The most well-defined and largest optical signals were obtained from the middle and hind legs during righting.

Peak ground reaction forces generated during righting were eight times greater than those produced during running (Table 1; Fig. 8). Righting forces oriented in the vertical direction with respect to the ground were nearly fourfold greater than those oriented horizontally (Table 1).

General utility of photoelastic technique

Since, during the righting behavior, the orientation of the middle and hind legs of the cockroach changed with respect to the body and to a particular location on the substratum, it is difficult to imagine obtaining single leg ground reaction force

Table 1. *Ground reaction forces*

Behavior	Vertical force (N)	Vertical force per unit body weight	Total horizontal force (N)	Horizontal force per unit body weight
Running	0.017±0.004	0.49±0.11	0.005±0.001	0.14±0.02
Righting	0.142±0.014	5.06±0.57	0.034±0.006	1.15±0.15

Measurements for running were made at a point during a step when the vertical force was maximized.

The total horizontal force is the component lying in the plane parallel to the ground surface, regardless of direction.

Values are mean ± S.E.M.; N=6 for running, N=8 for righting.

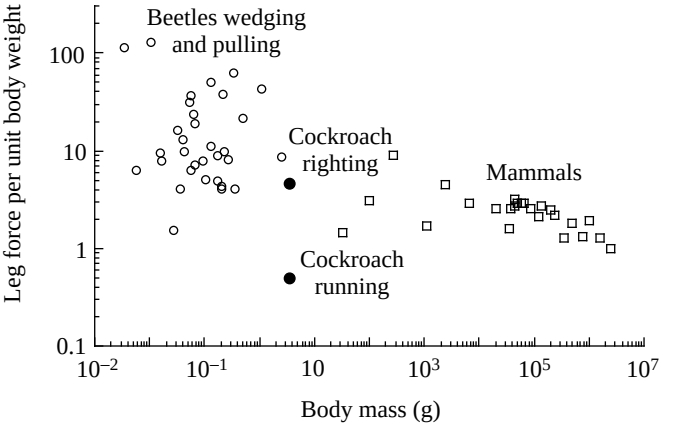

Fig. 9. Leg force per unit body weight as a function of body mass on logarithmic axes. The leg of a 3 g death-head cockroach generated substantially more force during righting than during running. The cockroach generated relative forces similar to those of many larger mammals (data from Alexander, 1985; Biewener *et al.* 1988*a*,*b*), but was at the low end of the range measured for wedging (data from Evans, 1977) and load-pulling beetles (data from Evans and Forsythe, 1984). Leg force per unit body weight was calculated by dividing the cumulative forces for all legs by the total number of legs involved in the activity.

measurements from a technique other than photoelastics. Modified force-platform techniques have been successful in determining single leg ground reaction forces during walking and running in a straight line (Blickhan and Barth, 1985; Full and Tu, 1990). However, the probability that a leg will contact a predictable location during more complex, less predictable, behaviors is simply too low. More importantly, a force plate cannot determine the forces produced by all the legs simultaneously. Attaching strain gauges to all the legs is another possibility, but is technically challenging (Blickhan and Barth, 1985; Blickhan *et al.* 1993; Clarac and Cruse, 1982; Klarner *et al.* 1986). Moreover, placing a strain gauge or other apparatus directly onto a leg would make the measurement of a three-dimensional ground reaction force vector difficult (Clarac and Cruse, 1982). The photoelastic technique permits measurement of the ground reaction forces of all legs simultaneously in three-dimensional space.

The use of gelatin photoelastics is not without disadvantages. Because the gelatin plate is filmed from above, with the animal between the plate and the camera, the optical pattern may be partially obscured by the animal's body. Division of optical patterns into quadrants invariably requires judgment by the experimenter. Force measurement suffers from two further drawbacks. First, each gelatin plate must be calibrated individually, because of the lack of uniformity of the gelatin preparations and its relatively short life span. Second, force calculations depend directly on estimates of contact areas. Measurement of foot and calibration element contact areas on small scales can be difficult. Finally, if dynamic behaviors are to be studied, a camera with a sufficient framing rate is required, since the 60 fields s^{-1} provided by standard video cameras is often inadequate (Biewener and Full, 1992). A computer system capable of capturing video frames, and image analysis software are also required.

All things considered, the photoelastic system is simple and inexpensive to set up. In particular, it proved to be useful for quick, qualitative assessment of animal force production. The system shows potential for the analysis of a variety of force-producing activities, since the gelatin can be molded into a variety of shapes (e.g. for examining the force produced during climbing over a step; Yamauchi *et al.* 1993).

Discussion

Single leg peak ground reaction forces produced by cockroaches during righting were eight times greater than those produced during running (Table 1; Full *et al.* 1991). The peak resultant force generated by a single leg during righting behavior was 5.1 times the body weight, compared with a value of only 0.49 times body weight during running. Clearly, the force-generating ability of the cockroach leg is dependent on the behavior examined and is not close to maximal during running.

Running

The relative magnitudes of single leg ground reaction forces during running determined in the present study were similar to those found previously using a force platform (Full *et al.* 1991; Table 1). The magnitudes of single leg forces relative to body weight during running were lower than in larger pedestrian vertebrates because of both the greater leg number and the longer leg contact time of smaller insects (Fig. 9; Blickhan and Full, 1993). Cockroaches using six legs distribute peak ground reaction forces among more legs than bipeds or quadrupeds. The peak force on a single cockroach leg is reduced by using a greater number of legs to contact the ground during running, because the average force over one cycle of leg movements must be equal to body weight. Cockroaches also distribute the ground reaction forces on a given leg over a relatively long period. Hexapedal (Ting *et al.* 1994) and octapedal (Blickhan *et al.* 1993) runners tend to have duty factors (β, the fraction of a stride period during which a leg is in contact with the ground) of 0.5 or above, even at relatively high speeds. By contrast, duty factors decrease with increasing speed in

quadrupedal mammals from 0.7 during a slow walk to 0.2 during asymmetrical galloping gaits (Alexander and Jayes, 1978). Peak leg ground reaction force (F) for quadrupeds ($F=0.15\pi mg/\beta$ for the forelegs and $F=0.10\pi mg/\beta$ for the hindlegs, where m is body mass) and bipeds ($F=\pi mg/4\beta$; Alexander *et al.* 1979) increases as duty factor decreases. We conclude that, in small arthropod runners, greater leg number and/or longer contact times can favor the reduction of the magnitudes of peak forces on individual legs.

Righting

The capacity of a single leg to generate force is more likely to be measured from righting behavior than from running in the death-head cockroach *B. discoidalis*. To investigate the magnitude of the leg forces produced during the righting behavior of cockroaches relative to predictions and data from other species, variation due to leg number, body mass and musculo-skeletal parameters must be considered.

The maximum force produced by the leg of a multi-legged animal should be less than that of an animal possessing fewer legs if both have a relatively similar percentage of body mass available with which to move their legs. At nature's extremes, this must be true. The relative force generated by a single leg of a giant millipede is likely to be less than that generated by a leg of an eight-legged crab, six-legged insect or four-legged lizard of the same body mass. It is less intuitive, however, whether the leg of a small six-legged insect generates more, or less, force per body weight than that of a two- or four-legged vertebrate. Assuming that each leg of an individual generates a similar maximum force, then each leg of an insect should account for approximately one-sixth of the total maximum force production, whereas that accounted for by a single leg of a quadruped or a biped would be one-quarter or one-half of the totals, respectively. This may account for the fact that a single *B. discoidalis* leg constitutes less than 2% of the total body mass (Full *et al.* 1994) compared with values of 9–23% measured for a single leg of a quadrupedal or bipedal vertebrate (Fedak *et al.* 1982).

If muscle force production scales geometrically, then the effect of mass more than compensates for the force reduction because of the greater leg number in insects compared with bipeds or quadrupeds. If force is proportional to cross-sectional area (including muscle cross-sectional area) and body mass is proportional to volume, then force per unit body weight would be expected to scale as mass$^{-0.33}$ for geometrically similar animals. Since body mass should decrease far more than cross-sectional area as body length decreases, mass-specific force production capacity should be greater for smaller animals. Alexander (1985) found that the maximum force generated per unit body weight for a wide variety of species and behaviors fell within limits defined by two functions (force/weight=$20m^{-0.33}$ and force/weight=$0.5m^{-0.33}$; where m is mass in kg) that varied by 40-fold at a given body mass. Although scaling maximum force per body weight to $m^{-0.33}$ between geometrically similar arthropods appears justifiable (Nachtigall, 1977; Manton, 1953; Evans, 1977), a broader comparison of pedestrian species suggests a much smaller exponent for m (see Fig. 1 in Alexander, 1985). Data for mammals suggest a force per weight *versus* body mass exponent of −0.1 or less (Alexander *et al.* 1981). Biewener (1989) showed that muscle mass-specific force production in quadrupedal mammals scales as $m^{-0.25}$, but effective mechanical advantage (i.e. the moment arm ratio which determines the relative magnitude of force needed to counteract the external force acting about a joint) scales as $m^{0.25}$. Even though small mammals can generate relatively greater muscle forces than larger mammals, small mammals operate at much lower effective mechanical advantages, resulting in a leg force production per unit body weight that is similar to quadrupedal mammals that differ by four orders of magnitude in body mass (i.e. an exponent closer to zero). Non-geometric scaling of leg force production per unit body weight (i.e. an exponent less negative than −0.33), therefore, along with greater leg number may aid in explaining why maximum relative leg force production in righting cockroaches, as well as in some other small insects, can be similar to values for vertebrates nearly 1000 times more massive (Fig. 9).

Leg number and body mass alone are insufficient to explain the variation observed in relative leg force production. Enormous diversity in musculo-skeletal parameters exists among animals. Our recalculations of single leg forces relative to body weight produced by the hind legs of wedging (Evans, 1977) and load-pulling (Evans and Forsythe, 1984) beetles show an almost 100-fold variation for insects ranging in mass from 3 mg to 3 g. Simple inspection of leg morphology reveals obvious differences in the percentage of muscle available. Evans and Forsythe (1984) found a four- to tenfold difference in mechanical advantage between fast-running and slow, strong burrowing beetles. Values for maximum leg force generation by death-head cockroaches relative to body weight were at the low end of the range of normalized, single leg forces calculated for insects (Evans, 1977; Evans and Forsythe, 1984; Fig. 9). Direct measurement of the relative leg force production in death-head cockroaches during wedging behavior (3.7 times body weight) as well as musculo-skeletal modeling estimates (4.8 times body weight; Full and Ahn, 1995) support the contention that the leg force production per unit body weight found in the present study for righting behavior (5.1±0.6) is near maximal. Although comparable performance tests have yet to be conducted on load-pulling, death-head cockroaches can be characterized as moderately strong force producers (force ratio=2.4–4.8; force ratio is the force/$W^{0.66}$, where W is body weight, depending on the number of legs pushing in synchrony), but relatively fast runners (velocity ratio=2, where the velocity ratio is the maximum velocity/$W^{0.33}$; Evans and Forsythe, 1984) compared with beetles. The most powerful burrowing beetles have force ratios as high as 60, and the fastest species have velocity ratios of over 6 (Evans and Forsythe, 1984).

Running versus *righting*

Cockroach leg forces were eight times greater during

righting than during running. This supports the hypothesis that relative leg forces produced during running and maximum leg force will differ more in small arthropods than in larger vertebrates. Maximal relative leg forces can be large in small insects, partly as a result of scaling. Observed values for running are low owing, in part, to their greater leg number. This difference has interesting implications for leg performance with respect to musculo-skeletal design, but much of the variation in musculo-skeletal parameters remains to be explained. Evaluation of pedestrian arthropod leg performance could benefit significantly from further measurement of force production during running and under conditions of maximal force production in the same species, together with measurements of muscle force production and effective mechanical advantage. We have begun to make these measurements in conjunction with the production of a three-dimensional musculo-skeletal leg model.

Supported by ONR Grant N00014-92-J-1250. We would like to thank Rodger Kram for his assistance.

References

ALEXANDER, R. MCN. (1985). The maximum forces exerted by animals. *J. exp. Biol*. **115**, 231–238.

ALEXANDER, R. MCN. AND JAYES, A. S. (1978). Vertical movements in walking and running. *J. Zool., Lond*. **185**, 27–40.

ALEXANDER, R. MCN., JAYES, A. S., MALOIY, G. M. O. AND WATHUTA, E. M. (1981). Allometry of the leg muscles of mammals. *J. Zool., Lond*. **194**, 539–552.

ALEXANDER, R. MCN., MALOIY, G. M. O., NJAU, R. AND JAYES, A. S. (1979). Mechanics of running of the ostrich (*Struthio camelus*). *J. Zool., Lond*. **187**, 169–178.

BENNET-CLARK, H. C. (1975). The energetics of the jump of the locust, *Schistocera gregaria*. *J. exp. Biol*. **63**, 53–83.

BIEWENER, A. A. (1989). Scaling body support in mammals: limb posture and muscle mechanics. *Science* **245**, 45–48.

BIEWENER, A. A., BLICKHAN, R., PERRY, A. K., HEGLUND, N. C. AND TAYLOR, C. R. (1988*a*). Muscle forces during locomotion in kangaroo rats: force platform and tendon buckle measurements compared. *J. exp. Biol*. **137**, 191–205.

BIEWENER, A. A. AND FULL, R. J. (1992). Force platform and kinematic analysis. In *Biomechanics: Structures and Systems, A Practical Approach* (ed. A. A. Biewener), pp. 45–73. Oxford: IRL Press at Oxford University Press.

BIEWENER, A. A., THOMASON, J. J. AND LANYON, L. E. (1988*b*). Mechanics of locomotion and jumping in the horse (*Equus*): *in vivo* stress in the tibia and metatarsus. *J. Zool., Lond*. **214**, 547–565.

BLICKHAN, R. AND BARTH, F. G. (1985). Strains in the exoskeleton of spiders. *J. comp. Physiol.* A **157**, 115–147.

BLICKHAN, R. AND FULL, R. J. (1993). Similarity in multilegged locomotion: Bouncing like a monopode. *J. comp. Physiol.* **173**, 509–517.

BLICKHAN, R., FULL, R. J. AND TING, L. (1993). Exoskeletal strain: evidence for a trot–gallop transition in rapidly running ghost crabs. *J. exp. Biol*. **179**, 301–321.

CLARAC, F. AND CRUSE, H. (1982). Comparison of forces developed by the leg of the rock lobster when walking free or on a treadmill. *Biol. Cybernetics* **43**, 109–114.

CRUSE, H. (1976). The function of the legs in the free walking stick insect, *Carausius morosus*. *J. comp. Physiol.* A **112**, 235–262.

DALLY, J. W. AND RILEY, W. (1991). *Experimental Stress Analysis.* New York: McGraw-Hill.

EVANS, M. E. G. (1977). Locomotion in the Coleoptera Adephaga, especially Carabidae. *J. Zool., Lond*. **181**, 189–226.

EVANS, M. E. G. AND FORSYTHE, T. G. (1984). A comparison of adaptations to running, pushing and burrowing in some adult Coleoptera: especially Carabidae. *J. Zool., Lond*. **202**, 513–534.

FEDAK, M. A., HEGLUND, N. C. AND TAYLOR, C. R. (1982). Energetics and mechanics of terrestrial locomotion. II. Kinetic energy changes of the limbs and body as a function of speed and body size in birds and mammals. *J. exp. Biol*. **79**, 23–40.

FULL, R. J. AND AHN, A. N. (1995). Static forces and moments generated in the insect leg – comparison of a three-dimensional musculo-skeletal computer model with experimental measurements. *J. exp. Biol*. **198**, 1285–1298.

FULL, R. J., BLICKHAN, R. AND TING, L. H. (1991). Leg design in hexapedal runners. *J. exp. Biol*. **158**, 369–390.

FULL, R. J., KRAM, R. AND WONG, B. (1994). Mechanical energies of swinging six legs. *Am. Zool.* **34**, 45A.

FULL, R. J. AND TU, M. S. (1990). The mechanics of six-legged runners. *J. exp. Biol*. **148**, 129–146.

FULL, R. J. AND TU, M. S. (1991). Mechanics of a rapid running insect: two-, four- and six-legged locomotion. *J. exp. Biol*. **156**, 215–231.

FULL, R. J. AND TULLIS, A. (1990). Capacity for sustained terrestrial locomotion in an insect: Energetics, thermal dependence and kinematics. *J. comp. Physiol*. B **160**, 573–581.

HARRIS, J. (1978). A photoelastic substrate technique for dynamic measurements of forces exerted by moving organisms. *J. Microscopy* **114**, 219–228.

HARRIS, J. AND GHIRADELLA, H. (1980). The forces exerted on the substrate by walking and stationary crickets. *J. exp. Biol*. **85**, 263–279.

HERREID II, C. F. AND FULL, R. J. (1984). Cockroaches on a treadmill: aerobic running. *J. Insect Physiol*. **30**, 395–403.

KATZ, S. L. AND GOSLINE, J. M. (1993). Ontogenetic scaling of jump performance in the African desert locust (*Schistocerca gregaria*). *J. exp. Biol*. **177**, 81–111.

KLARNER, D. B., KLARNER, D. AND BARNES, W. J. P. (1986). The cuticular stress detector (CSD2) of the crayfish. II. Activity during walking and influences on leg coordination. *J. exp. Biol*. **122**, 161–175.

MANTON, S. M. (1953). Locomotory habits and the evolution of the larger arthropodan groups. *Symp. Soc. exp. Biol*. **7**, 339–353.

NACHTIGALL, W. (1977). Swimming mechanics and energetics of locomotion of variously sized water beetles – Dytiscidae, body length 2–35 mm. In *Scale Effects in Animal Locomotion* (ed. T. J. Pedley), pp. 269–283. London: Academic Press.

QUEATHEM, L. AND FULL, R. J. (1995). Variation in jump force production within an instar of the grasshopper *Schistocerca americana*. *J. Zool., Lond.* **235**, 605–620.

TING, L. H., BLICKHAN, R. AND FULL, R. J. (1994). Dynamic and static stability in hexapedal runners. *J. exp. Biol*. **197**, 251–269.

YAMAUCHI, A., WONG, B., KRAM, R. AND FULL, R. J. (1993). Strategy of scaling steps in insects. *Am. Zool*. **33**, 29A.